Electromagnetic Heat-induced of Nanowire in Liquid: Computation of the Bubble Shape

A. Chaari, T. Grosges, L. Giraud-Moreau, and D. Barchiesi
Project Group for Automatic Mesh Generation and Advanced Methods
Gamma3 Project (UTT-INRIA), University of Technology of Troyes, France

Abstract— The computation of the temperature with accuracy is essential to determine the shape of a bubble around a nanowire immersed in a liquid. The study of the physical phenomenon consists in solving a coupled photo-thermic system between light and nanowire. The numerical multiphysic model is developped to study and simulate the variations of the temperature and the shape of the induced bubble after the illumination of the nanowire. An optimized finite element method, including adaptive remeshing scheme, is developped and used to solve the problem. The evolution of the bubble is achieved by taking into account the physical and geometrical parameters of the nanowire. The feedback relation between the sizes and shapes of the bubble and nanowire is deduced.

1. INTRODUCTION

Many researchers are interested by the use of nanomaterials. Usually used materials in the chemical industry and in manufactures of nanotubes and nanowires are TiO_2 and ZnO [1–3]. The use of such nanomaterials (natural or artificial) increases and these are dispersed in air or in water [4]. The investigation on their impacts on the environment and health becomes a necessity (e.g., toxicity analysis) [5] and the detection of the presence of such nanomaterials in the environment becomes crucial. These detections of such a nanowire/nanotube can be achieved through two modes. The first mode consists in a direct detection of the nanowire by the measurement of the scattering of light emitted by the nanomaterial through optical microscopy. Such a detection mode must be difficult due to a weak signal/noise ratio. A second mode consists in an indirect method by studying the bubble created by the photo-thermal response of the illuminated nanowire immersed in the liquid. In that approach, the nanowire absorbs the electromagnetic radiation (energy), heats and induces the creation of a nanobubble [6, 7] for temperature exceeding the vaporization threshold of the liquid. The detection is achieved after the grow of the created bubble and the morphology of the nanowire is studied from the analysis of the shape and size of the bubble. Therefore, the problem consists in solving a photo-thermic coupled system (light, nanowire and heat) taking into account the physical parameters of the system (i.e., permittivity and conductivity of materials, wavelength and power of the laser).

In that context, a numerical multiphysic model is developped in order to analyse the behavior of the nanowires under illumination by a incident laser. The formation of the bubble, associated to the nanowire of TiO_2 immersed in water and illuminated by a laser pulse, is studied. An optimization process, including adaptive remeshing scheme, is used to detect the variations of the temperature, the bubble shape evolution and ensuring the convergence of the solution to the physical solution [8–10]. The paper is organized as follows: Section 2 describes the model and the numerical resolution method. In Section 3, the results of numerical simulations are presented before concluding.

2. MODEL AND FEM FORMULATION

Finite Element Method (FEM) has proved to be an efficient method for the computation of electromagnetic field around nanostructures [11]. The main advantages of the FEM are first its ability to treat any type of geometry and material inhomogeneity (with complex permittivity) [11], second the control of the accuracy of computation to evaluate accuracy of solutions, by using a non regular mesh of the domain of computation and remeshing process.

The PDE system is formed of the Helmholtz' for non-magnetic material with harmonic time dependence, and the Poisson's equations (the stationary heat equation, coupled by a source term in the second one [12]:

$$\left[\nabla \cdot \left(\frac{1}{\epsilon_r(x,y)}\nabla\right) + \frac{\omega^2}{c^2}\right] H_z(x,y) = 0 \tag{1}$$

$$\left[\nabla \cdot (\kappa(x,y)\nabla)\right] T(x,y) + \frac{\omega\epsilon_0 \mathrm{Im}(\epsilon_r(x,y))}{2} \left|\mathbf{E}(x,y)\right|^2 = 0, \tag{2}$$

where ∇ is the differential vector operator, in cartesian coordinates, $\cdot$ is the scalar product, c is the speed of light in vacuum, ω the angular frequency of the monochromatic wave, $\kappa(x, y)$ the thermal conductivity, $\epsilon_r(x, y)$ the relative permittivity of media and ϵ_0, the permittivity of vacuum. The shape of the nanowire is defined in the (x, y) plane, as the electric field $\mathbf{E}(x, y)$ which is deduced from the magnetic field $H(x, y)$ along z direction, through the Maxwell-Ampere's equation. The boundary conditions result from the integration of the PDE and from the flux continuity [13]:

$$\mathbf{n}_{12} \cdot \left[\left(\frac{1}{\epsilon_2} \nabla H_2 \right) - \left(\frac{1}{\epsilon_1} \nabla H_1 \right) \right] = 0 \quad \text{and} \quad \mathbf{n}_{12} \cdot [(\kappa_2 \nabla T_2) - (\kappa_1 \nabla T_1)] = 0 \tag{3}$$

where $\mathbf{n}_{12}$ is the normal to the boundary vector, ϵ_l ($l = 1, 2, 3$) are the complex permittivity and κ_l the thermal conductivity of the nanowire, vapor and water medium respectively. The electromagnetic boundary condition (Equation (3)) in 2D geometries, is formally equivalent to the continuity of the tangential component of the electric field. The boundary conditions on the fictitious external boundary of the domain of computation (water), corresponding to the free propagation of the diffracted field $H_3 - H_i$ [13] and the incoming illumination H_i, are defined by:

$$\mathbf{n}_{23} \cdot [(\nabla H_3)] = \jmath \, [\mathbf{k} \cdot \mathbf{n}] \, \vec{H}_i + \jmath \frac{\omega}{c} (H_3 - H_i) \quad \text{and} \quad T_3 = T_0, \tag{4}$$

where H_i is the illuminating monochromatic, lying along y, magnetic field: $H_i = H_i^0 \exp(\jmath\omega t - \jmath\mathbf{k} \cdot \mathbf{r})$, with $\mathbf{k} = (0, \omega/c, 0)$, the wave vector, and $\jmath$ the square root of -1. The solution of this FEM formulation, including a improved remeshing procedure, has been checked and compared with rigorous Mie theory [10, 14, 15].

The resolution of the coupled electromagnetic and heat problems allows to extract the spatial distribution of the temperature in the computational domain. From the map of temperature and for a fixed threshold of vaporization α, the identification of the shape and size of the bubble around the nanowire can be achieved. Such informations on shape and size of the bubble would be used to construct a relation between the geometric characteristics of the bubble and the nanowire.

3. NUMERICAL RESULTS AND DISCUSSION

We consider a TiO_2 elliptical nanowire of semi-axes ($a = 45$ nm, $b = 10$ nm), with thermal conductivity $\kappa(TiO_2) = 11.7\,\mathrm{W m^{-1} K^{-1}}$ immersed in water ($\epsilon_r(\text{water}) = 1.79$, $\kappa(\text{water}) = 0.6\,\mathrm{W m^{-1} K^{-1}}$) at temperature $T_0 = 25°$C (298.15 K). The nanowire is illuminated by a TM-polarized laser pulse at wavelength $\lambda = 1050$ nm of complex permittivity $\epsilon_r(TiO_2)_{1050} = 5.4600 + \jmath 0.00148$ with a power density per area units $P_S = 1.75 \times 10^{12}\,\mathrm{W/m^2}$ [16, 17]. The materials of the system are considered isotropic and homogeneous.

The results of the adaptive process on mesh and on the temperature maps are illustrated on Figure 1. Figures 1(a), (d) show the initial mesh M_0 and the associated temperature. The adaptive process on the temperature field T produces the mesh M_T and the temperature map (see Figures 1(b), (e), respectively). The mesh is adapted on the outline of the nanowire that presents strong variations of the temperature. For a water vaporization threshold $\alpha = 100°$C (373.15 K), the detection of the new material (water vapor) is obtained from the temperature map computed on the mesh M_T. The Figure 1(c) presents the areas of the three materials: TiO_2 (red), vapor (green) and water (blue). The computation of the temperature on the domain that contains the water vapor requires to include the physical parameters of the vapor (permittivity $\epsilon_r(\text{vap}) = 1.79$ and thermal conductivity $\kappa(\text{vap}) = 0.05\,\mathrm{W m^{-1} K^{-1}}$). The spatial distribution of the temperature field T on the mesh M_{V_0} after detection of the bubble produced around the nanowire is shown on Figure 1(e). The final mesh M_F is obtained, after eight iterations, by applying the adaptive process on the field T taking into account the bubble. That mesh is adapted in the bubble especially on its outline where variations in the temperature occur and relaxed inside the nanowire where the temperature is almost constant (Figure 1(c)). The remeshing process takes into account the shape and size of the bubble. The Figure 1(f) shows the temperature map T on the mesh M_F after convergence to a stable solution. The level curves are smooth where a strong variation of the temperature is shown (in the vicinity of the boundary of the bubble and the nanowire). The map also shows an increase of the temperature in the nanowire due to the creation of the bubble. This increase is due to the diffusion of the temperature, produced by the nanowire after detection of the bubble (i.e., the water vapor has a smaller thermal conductivity than water).

To study the evolution of the shape and size of the bubble, we also consider the nanowire illuminated for various wavelengths ($\lambda = 950$ nm, $\lambda = 1000$ nm and $\lambda = 1050$ nm) with adapeted physical

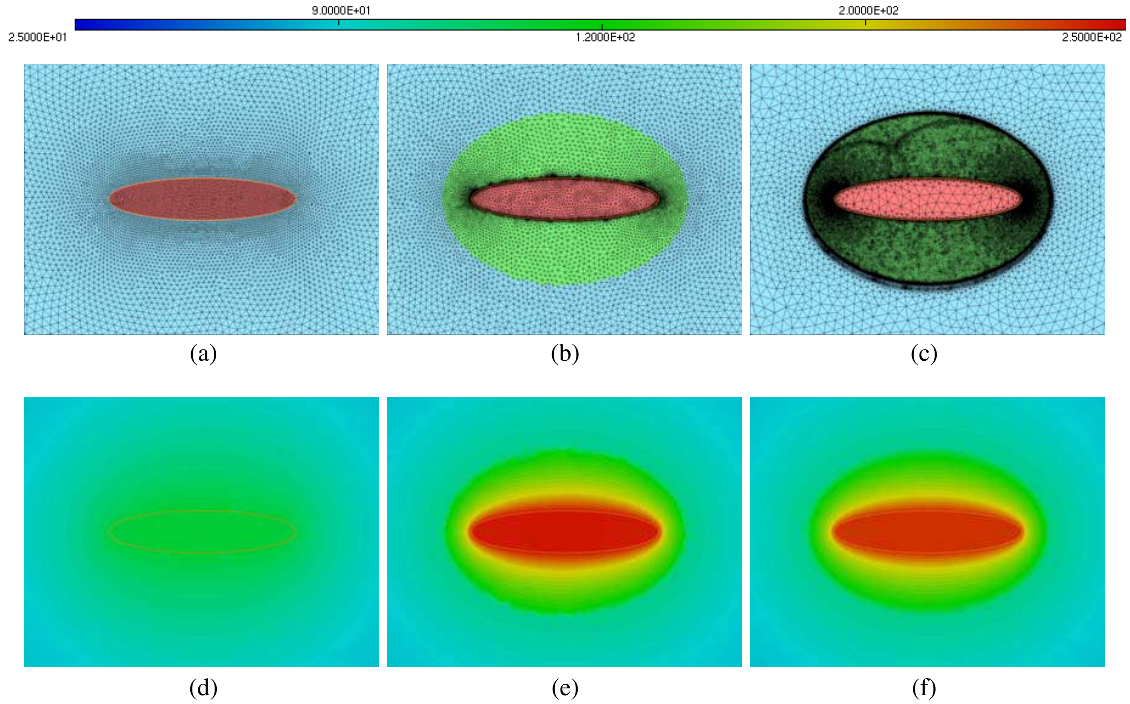

Figure 1: Meshes and temperature fields for nanowire illuminated at $\lambda = 1050\,\text{nm}$: (a) Initial mesh M_0, (c) adaptive mesh M_{V_0}, (e) M_F and the associated temperature maps on (b) M_0, (d) M_{V_0} and (f) M_F.

parameters ($\epsilon_r(\text{TiO}_2)_{950} = 5.500 + j0.00164$, $\epsilon_r(\text{TiO}_2)_{1000} = 5.475 + j0.00154$ and $\epsilon_r(\text{TiO}_2)_{1050} = 5.460 + j0.00148$). For λ increasing, the imaginary part of the complex permittivity of the TiO_2 decreases, leading to a decrease of the energy absorbed by the nanowire. Therefore, the temperature also decreases and the shape and size of bubble are changing. The Figure 2(a) shows the evolution of the aspect ratio of the bubble $R_{\text{bubble}} = A/B$ (A and B being the semi-axes of the bubble) as function of the aspect ratio of the nanowire R_{nanowire} for the three wavelengths. From the computed data, a function F, satisfying $R_{\text{bubble}} = F(R_{\text{nanowire}})$, can be obtained through a nonlinear least-squares fit method (LLS) by the Marquardt-Levenberg algorithm [18, 19]. The method is used to find a set of the best parameters fitting the data. It is based on the sum of the squared differences or residuals (SSR) between the input data and the function evaluated at the data. The applied algorithm consists in minimizing the residual variance $\hat{\sigma}^2 = \text{SSR}/\text{NDF}$ with NDF the number of degrees of freedom (number of the data points (NDP) minus number of the estimated parameters) after a finite number of iterations (FNI). Therefore, the function can be written as follows:

$$R_{\text{bubble}} = F\left(R_{\text{nanowire}}\right) = c_0 + \frac{c_1}{\left(R_{\text{nanowire}} - c_2\right)^2}, \tag{5}$$

with c_0, c_1 and c_2 are set of parameters varying as function of the wavelength. The parameter c_0 concerns the asymptote value which is related to the maximum ratio for a circular bubble, c_1 is the inverse of the decay rate of the function F which is related to the speed tending to the circular shape and c_2 is the initial ratio from which the bubble begins to form. Table 1 shows the fit parameters for each wavelength. The F function is continuous and strictly decreasing for R_{nanowire} in the interval $]c_2, +\infty[$, therefore the inverse function F^{-1} exists. The measurement of the aspect ratio of the bubble R_{bubble} allows to predict the aspect ratio of the nanowire R_{nanowire} through the relation: $R_{\text{nanowire}} = F^{-1}(R_{\text{bubble}})$. Figure 2(b) presents the evolution of the bubble volume (in 2D: $V_{\text{bubble}} = \pi AB$) as function of the volume of the nanowire (i.e., $V_{\text{nanowire}} = \pi ab$) for each wavelength. From the computed data (vapor bubble for each nanowire and for each wavelength) and by using the same method and the same algorithm a function G can be obtained through a fit. That function G allows to obtain the relation between the volumes ($\ln(V_{\text{bubble}}) = G(\ln(V_{\text{nanowire}}))$. The G function is continuous and strictly increasing, therefore the inverse function G^{-1} also exists. The measurement of the bubble volume V_{bubble} can be used to determine the volume of the nanowire V_{nanowire} through the relation $\ln(V_{\text{nanowire}}) = G^{-1}(\ln(V_{\text{bubble}}))$. With the two functions F^{-1} and

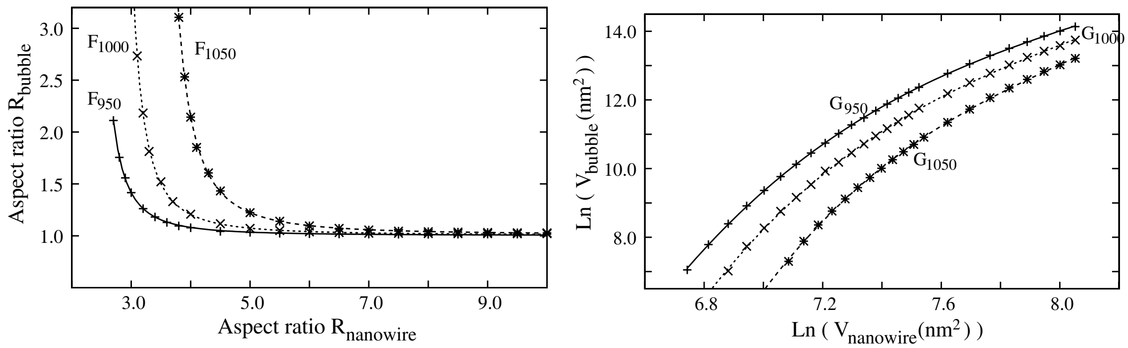

(a) (b)

Figure 2: Evolution of (a) the aspect ratio of the bubble R_{bubble} as function of the aspect ratio of the nanowire R_{nanowire} for the three wavelengths and (b) evolution of the volume of the bubble V_{bubble} as function of the volume of the nanowire V_{nanowire}.

Table 1: Fit parameters of the F function.

λ	NDP	NDF	$\hat{\sigma}^2$	Set of parameters			FNI
				c_0	c_1	c_2	
950	42	39	1.8111e-5	1.0036	0.2418	2.2334	32
1000	38	35	5.5850e-5	1.0082	0.3659	2.6394	15
1050	31	28	1.1106e-4	1.0124	0.6529	3.2416	23

G^{-1} the size and shape of the nanowire can be obtained from the information on the bubble:

$$\ln(V_{\text{nanowire}}) = \ln\left(\pi b^2 F^{-1}(R_{\text{bubble}})\right) = G^{-1}\left(\ln(V_{\text{bubble}})\right), \tag{6}$$

consequently,

$$b = \left[\frac{\exp(G^{-1}\left(\ln(V_{\text{bubble}})\right))}{\pi F^{-1}(R_{\text{bubble}})}\right]^{1/2} \quad \text{and} \quad a = \left[\frac{F^{-1}(R_{\text{bubble}})\exp\left(G^{-1}(\ln(V_{\text{bubble}}))\right)}{\pi}\right]^{1/2}. \tag{7}$$

Therefore the measurement of the size and shape of the bubble can be used to obtain information on the geometry of the nanowire and to reconstruct the size and shape of the nanowire.

4. CONCLUSION

The paper focus on the forming and the evolution of the shape and size of the bubble through a photo-thermal process between a nanowire of TiO_2 immersed in water and an electromagnetic wave. The increase of temperature is related to the geometry of the nanowire which leads to an increase in the shape and size of the bubble. That solution is computed by developing an adaptive remeshing method to computed with accuracy the temperature and by adapting the mesh to the evolution of the bubble. The coupled problem light-matter and heat is solved through an adaptive loop process allowing to converge to a stable solution and to decrease the number of nodes. The influence of the laser source and the geometrical parameters (wavelength, size and shape of the nanowire) related to the size and shape of the bubble are presented and analyzed. The aspect ratio and the volume of the bubble can be expressed as function of the aspect ratio and the volume of the nanowire. By solving the inverse problem two functions are obtained enabling to find the size and shape of the nanowire from the size and shape of bubble.

ACKNOWLEDGMENT

The authors thank the ANR-2011-NANO-008 NANOMORPH for financial support.

REFERENCES

1. Boroski, M., A. C. Rodrigues, J. C. Garcia, L. C. Sampaio, J. Nozaki, and N. Hioka, "Combined electrocoagulation and TiO_2 photoassisted treatment applied to wastewater effluents from

pharmaceutical and cosmetic industries original," *J. Hazard. Mater.*, Vol. 162, No. 1, 448–454, 2009.

2. Chatterjee, D. and A. Mahata, "Demineralization of organic pollutants on the dye modified TiO_2 semiconductor particulate system using visible light original," *Appl. Catal. B — Environ.*, Vol. 33, No. 2, 119–125, 2001.
3. Karamanis, D., A. N. Okte, E. Vardoulakis, and T. Vaimakis, "Water vapor adsorption and photocatalytic pollutant degradation with TiO_2-sepiolite nanocomposites original," *Appl. Clay Sci.*, Vol. 53, No. 2, 181–187, 2011.
4. Bystrzejewska-Piotrowska, G., J. Golimowski, and P. L. Urban, "Nanoparticles: Their potential toxicity, waste and environmental management," *Waste Manage.*, Vol. 29, No. 9, 2587–2595, 2009.
5. Nowack, B., "The behavior and effects of nanoparticles in the environment," *Environ. Pollut.*, Vol. 157, No. 4, 1063–1064, 2009.
6. Lapotko, D. and E. Lukianova, "Laser-induced micro-bubbles in cells," *Int. J. Heat Mass Transfer*, Vol. 48, No. 1, 227–234, 2005.
7. Lapotko, D., E. Lukianova, and A. Shnip, "Photothermal responses of individual cells," *J. Biomed. Opt.*, Vol. 10, No. 1, 014006, 2005.
8. Barchiesi, D., T. Grosges, E. Kremer, and M. L. de la Chapelle, "Electromagnetic heat induced in meso-structures: Computation of temperature in metallic dimers," *PIERS Online*, Vol. 7, No. 5, 406–410, 2011.
9. Chaari, A., L. Giraud-Moreau, T. Grosges, and D. Barchiesi, "Numerical modeling of the photothermal processing for bubble forming around nanowire in a liquid," *Sci. World J.*, Vol. 2014, No. 794630, 2014.
10. Grosges, T., H. Borouchaki, and D. Barchiesi, "New adaptive mesh development for accurate near-field enhancement computation," *J. Microsc.*, Vol. 229, No. 2, 293–301, 2008.
11. Grosges, T., S. Petit, D. Barchiesi, and S. Hudlet, "Numerical modeling of the subwavelength phase-change recording using an apertureless scanning near-field optical microscope," *Opt. Express*, Vol. 12, No. 24, 5987–5995, 2004.
12. Baffou, G., C. Girard, and R. Quidant, "Mapping heat origin in plasmonic structures," *Physical Review Letters*, Vol. 104, No. 13, 136805, 2010.
13. Jin, J., *The Finite Element Method in Electromagnetics*, John Wiley and Sons, New York, 1993.
14. Grosges, T., A. Vial, and D. Barchiesi, "Models of near field spectroscopic studies: Comparison between finite element and finite difference methods," *Opt. Express*, Vol. 13, No. 21, 8483–8497, 2005.
15. Grosges, T., H. Borouchaki, and D. Barchiesi, "Improved scheme for accurate computation of high electric near-field gradients," *Opt. Express*, Vol. 15, No. 3, 1307–1321, 2007.
16. Brown, T. L. and J. A. Rice, "The effect of laser wavelength and power density on the laser desorption mass spectrum of fulvic acid," *Org. Geochem.*, Vol. 31, No. 7–8, 627–634, 2000.
17. O'Connor, K., O. Morris, and E. Sokell, "Angular and energy distribution of Sn ion debris ejected from a laser-produced plasma source, for laser power densities in the range suitable for extreme ultraviolet lithography," *J. Appl. Phys.*, Vol. 109, No. 7, 073301, 2011.
18. Gill, P. E. and W. Murray, "Algorithms for the solution of the nonlinear least-squares problem," *SIAM J. Numer. Anal.*, Vol. 15, No. 5, 977–992, 1978.
19. Vasin, V. V. and G. Y. Perestoronina, "The Levenberg-Marquardt method and its modified versions for solving nonlinear equations with application to the inverse gravimetry problem," *Proc. Steklov Inst. Math.*, Vol. 280, No. 1, 174–182, 2013.